POLITECNICO DI TORINO
Repository ISTITUZIONALE

A FULLY IMPLICIT MATERIAL RESPONSE CODE WITH ABLATION AND PYROLYSIS FOR SIMULATION OF THERMAL PROTECTION SYSTEMS

(Article begins on next page)

04 August 2020

A FULLY IMPLICIT MATERIAL RESPONSE CODE WITH ABLATION AND PYROLYSIS FOR SIMULATION OF THERMAL PROTECTION SYSTEMS

Alessandra Dal Bianco[*1], **Domenic D'Ambrosio**[1], and **Vincenzo Mareschi**[2]

[1]*Politecnico di Torino, Dipartimento di Ingegneria Meccanica e Aerospaziale, 10129 Torino, Italy*
[2]*Thales Alenia Space Italia S.p.A., 10146 Torino, Italy*

ABSTRACT

The purpose of this paper is to introduce and describe a 2-D fully implicit numerical simulation tool capable of evaluating the behaviour of an ablative charring thermal protection system during atmospheric entry. In particular, the computational tool can model the heat transfer inside a solid porous material and the decomposition of the latter, pyrolysis gas density, pressure and speed distributions and surface recession. The governing equations are fully coupled and are integrated using a time-implicit scheme. The grid can contract to simulate the recession phenomenon and the recession rate can be evaluated using different ablation models, depending on the problem and on the available data. Spatial and temporal convergence tests demonstrated that the tool is second order accurate in space and time and comparisons with available numerical results are shown here for code verification.

Key words: aerothermodynamics; ablation; material thermal response.

1. INTRODUCTION

During atmospheric entry, the large kinetic energy of a space vehicle is converted, through a bow shock wave, into internal energy, generating a zone, especially close to the nose, where temperature is extremely high and gaseous species are in thermochemical non-equilibrium. Therefore, a heat shield is necessary to protect the spacecraft's substructure against intense heat fluxes from the gas to the vehicle. The accurate prediction of the thermal response of the TPS (Thermal Protection System) is essential to accurately design the heat shield with the aim of optimizing its thickness and shape.

Some thermal protection systems are made up of materials called ablative, that lose mass when subjected to high thermal loads. There can be different causes of mass loss such as phase change, chemical reactions and erosion, depending on the type of ablative material. In addition, some type of ablators, called charring ablators, undergo a pyrolysis process that involves the decomposition of the matrix and the generation of pyrolysis gas. The ablation products, that include char and pyrolysis gas, are then partially injected into the boundary layer bringing several beneficial effects to the heat shield, including the heat flux reduction.

Initial research concerning the numerical modelling of ablative TPS dates back to the late 1960s [MR68] and continued in the early 1970s [Cla73]. Then, looking at the literature, the interest faded for almost fifteen years, but it renewed in the late 1990s with studies mainly conducted at the NASA Ames Research Center that led to the development of the FIAT (Fully Implicit Ablation and Thermal Analysis Program) code [CM99], a numerical tool that can simulate the thermal response of ablators in a fully implicit way. Successively, the FIAT code was extended to two-dimensions through the development of the TITAN program (Two-dimensional Implicit Thermal Response and Ablation Program) [CM01] and to three-dimensions with 3dFIAT [CM05b, CMG10]. These simulation tools can also take into account the recession phenomenon using contracting computational grids.

A contracting grid scheme based on the work by Blackwell and Hogan [BH94, Bla88] was also implemented by Amar et al. [Ama06, ABE08, ABE09] in a numerical simulation tool capable of simulating the transient thermal response of an ablator with decomposition and gas pressure effects in one-dimension. An extension to three-dimensions was also presented by Amar and co-authors at NASA Johnson Space Center [ACK11], but the published results only described verification exercises carried out using manufactured solutions and the capability of dealing with recession still had to be tested.

The simulation tools mentioned above can only be weakly coupled with the external flow solutions. In practice, a CFD solution is separately computed and used as a boundary condition for the material response code, whose results (in particular the shape changes, the wall temperature distribution and the blowing gas mass fluxes) are then used as a boundary condition for the CFD solver. Recently, most research about TPS aims at developing a coupled CFD/material response code in order to improve the accuracy of the results. In particular, Martin and Boyd [MB08, MB09a, MB09b, MB10], coupled a one-dimensional material response implicit solver based on the CVFEM to LeMANS, a CFD code for the sim-

---

[*]Presently at Agilent Technologies Italia S.p.A., Leinì (TO), Italy

ulation of weakly ionized hypersonic flows. The one-dimensional code solves the governing equations for the ablator along normal lines with respect to the wall. It can simulate surface ablation and pyrolysis within the thermal protection system [MB08] and uses a contracting grid scheme to move the mesh. Very recently, further work by Martin's group at the University of Kentucky led to the implementation of a multi-dimensional material response solver [WM14].

In this paper, we describe the development and verification of a multi-dimensional thermal response and ablation code based on a finite volume method. The governing equations are solved using a a fully implicit time integration scheme. The resulting sparse matrix inversion is carried out through a preconditioned GMRES method. The code is capable of handling several degrees of complexity, depending on the material and on the desired computational cost of the simulation. In addition to inner decomposition, pyrolysis effects within a porous charring ablator can be studied, including in-depth gas flow, porosity and pore pressure. This information can be used to predict in-depth damage or mechanical removal caused by large pressure gradients inside the pore spaces. It has to be noted that steep pressure gradients caused by an intense production of pyrolysis gas have to be modeled with particular attention in order to avoid numerical instabilities that arise due to the different orders of magnitude of the variables involved in the process. Finally, the numerical simulation tool described here is also able to simulate the recession of the material using a contracting grid scheme as presented in Blackwell's work [BH94] and different ablation models can be used to evaluate the recession rate at the wall. The material response code is already fully coupled with a CFD solver. The resulting simulation tool includes the complementary contraction of the solid and fluid mesh, so that fluid dynamics and material response solutions can be obtained simultaneously, but in this paper we will show only results where the material response code is used in stand-alone mode, as the thermo-chemical modelling of gas/surface interactions has not been validated yet.

2. GOVERNING EQUATIONS

The governing equations for a porous charring ablator include a solid/gas phase energy equation and a number of continuity equations that depends on the amount of decomposing components and, possibly, on the presence of pyrolysis gas [Ama06]. The pyrolysis gas species are usually free to react among themselves, with the solid through erosion or coke phenomena, and with external atmospheric gases once they have escaped from the solid. However, in this work the pyrolysis gases are supposed to be a single non-reactive species in thermochemical equilibrium with the solid phases as described in previous works [Ama06, ABE08, ABE09]. The hypothesis of thermal equilibrium between the gaseous and the solid phases results in a single energy equation, and in a single temperature, for the whole ablating material. Under these assumptions, the model is illustrated through the following governing equations [Ama06]:

$$\frac{\partial}{\partial t}\int_v E_a dV - \int_s E_a \mathbf{v}_s \cdot \mathbf{n}dS + \int_s \phi\rho_g h_g \mathbf{v}_g \cdot \mathbf{n}dS$$
$$+ \int_s \dot{\mathbf{q}} \cdot \mathbf{n}dS = 0 \quad (1)$$

$$\frac{\partial}{\partial t}\int_v \rho_{s_i} dV - \int_s \rho_{s_i} \mathbf{v}_s \cdot \mathbf{n}dS = \int_v \dot{m}_{s_i} dV \quad (2)$$

$$\frac{\partial}{\partial t}\int_v \phi\rho_g dV - \int_s \phi\rho_g \mathbf{v}_s \cdot \mathbf{n}dS + \int_s \phi\rho_g \mathbf{v}_g \cdot \mathbf{n}dS$$
$$= \int_v \dot{m}_g dV \quad (3)$$

The three equations above govern the rate of change of the solid/gas phase energy, of the solid phase components density and of the gas phase density, respectively. The gas velocity $\mathbf{v}_g$ is found using the generalized multi-dimensional form of the Darcy's Law [Dar56, Whi86, NB06], the classical simplest form of the momentum equation for porous media:

$$\mathbf{v}_g = -\frac{\kappa\left(\beta\right)}{\phi\left(\beta\right)\mu\left(T\right)}\nabla p \quad (4)$$

In Eq. (4) the permeability, κ, is scalar, for we assume medium isotropy, and β is the extent of reaction that describes the partially charred zone in an ablative material:

$$\beta = \frac{\rho_v - \rho_s}{\rho_v - \rho_c} \quad (5)$$

Other authors [MB08, MB09a, MB09b] used an extended form of the Darcy's law, the so-called Forchheimer equation [NB06] that contains an additional quadratic drag term that becomes important when the gas speed is sufficiently high so that that the form drag due to solid obstacles is comparable to the surface drag due to friction[NB06].

The pressure distribution is obtained under the hypothesis that the thermodynamic state of the pyrolysis gas can be described by the perfect gas law:

$$p = \rho_g \frac{\mathcal{R}}{\mathcal{M}_g(T)}T \quad (6)$$

where the molecular mass of gas, $\mathcal{M}_g$, can vary with temperature.

Finally, the porous material energy E_a is defined in terms of pyrolysis gas and solid components energy:

$$E_a = \phi\rho_g e_g + \rho_v\left(1 - \beta\right)e_v + \rho_c\beta e_c \quad (7)$$

To determine the solid density variation due to the pyrolysis process, we assume a three-components decomposition model, since the phenolic resin usually undergoes a two-stage decomposition process [Gol65], while the filler remains unchanged. This peculiar behaviour of

Table 1. Coefficients in Eq. (10) for Carbon-Phenolic[Ama06], PICA[TJR$^+$96] and SLA 561v[TPS05]

	[units]	Carbon-Phenolic			PICA			SLA 561v
		A	B	C	A	B	C	A
ρ_{v_i}	[kg/m^3]	973.12	324.37	1560.19	228.26	973.12	160.18	232
ρ_{c_i}	[kg/m^3]	518.99	0	1560.19	0	792.92	160.18	128
k_i	[s^{-1}]	$4.48 \cdot 10^9$	$1.40 \cdot 10^4$	-	$1.40 \cdot 10^4$	$4.48 \cdot 10^9$	-	$5.02 \cdot 10^8$
ψ_i		3	3	-	3	3	-	3
E_i/R	[K]	20444.444	8555.556	-	8555.556	20444.444	-	19000
T_{min}	[K]	333.333	555.556	-	555.556	333.333	-	588.889

the carbon phenolic material allows the phenolic resin to be modelled as if it consists of two different components, ρ_A and ρ_B, that decompose separately. On the other hand, the filler has a constant density, ρ_C. Considering the previous assumptions, the solid density of the composite is given by[Ama06]:

$$\rho_s = \Gamma \left(\rho_A + \rho_B \right) + \left(1 - \Gamma \right) \rho_C \qquad (8)$$

The parameter Γ is defined as the volume fraction of resin inside the ablative material and it is an input constant. The total density of the charring ablator is given by[Ama06]:

$$\rho = \rho_s + \phi \rho_g \qquad (9)$$

We model the decomposition process through the Arrhenius relation:

$$\frac{\partial \rho_{s_i}}{\partial t} = \dot{m}_{s_i} = -k_i \rho_{v_i} \left(\frac{\rho_{s_i} - \rho_{c_i}}{\rho_{v_i}} \right)^{\psi_i} e^{\frac{E_i}{RT}} \qquad (10)$$

The coefficients appearing in Eq. (10) are listed in Table 1 for some typical ablative materials.

The resin decomposition generates pyrolysis gas in the pores space, so that the gas source term in Eq. (3) is given by:

$$\dot{m}_g = -\dot{m}_s = - \left[\Gamma \left(\dot{m}_A + \dot{m}_B \right) + \left(1 - \Gamma \right) \dot{m}_C \right] \qquad (11)$$

3. BOUNDARY CONDITIONS

Several types of surface boundary conditions can be selected depending on the available information. In particular, each time step may have a corresponding wall temperature distribution, or a surface energy balance could be solved in order to obtain the wall temperature. A simplified form of the surface energy balance equation is

$$\dot{q}_{conv} + \alpha \dot{q}_{rad} - \dot{q}_{cond} - \epsilon \sigma T_w^4 = 0 \qquad (12)$$

In Eq. (12) we neglect any chemical flux entering the surface as well as the pyrolysis and char products energy rates, as in the work by Dec and Braun [DB06]. The simplification is due to the difficulty in obtaining the thermochemistry tables needed to compute char and gas ablation rates and wall enthalpy. Of course, when the thermal response solver is coupled with the computational fluid dynamics solver, the surface energy balance equation will be written with the inclusion of the missing terms, which will be directly available from the coupled simulation of the external flow. The first and the second terms in Eq. (12) represent the convective and radiative heat fluxes absorbed by the surface, respectively, while the remaining two terms refer to the charring ablator contributions. Equation (12) is solved using the Newton-Raphson method at each time step and each boundary cell surface with the objective of obtaining the wall temperature. In addition, each time step requires a corresponding wall pressure distribution to provide a boundary condition to the pyrolysis gas continuity equation.

4. ABLATION MODEL

In certain atmospheric conditions, surface recession is barely detectable. In this case, it is possible to ignore the recession phenomenon, assuming that the grid remains unchanged during the simulation. However, when the ablation phenomenon has to be taken into account, our simulation tool can predict the material recession either specifying the recession rate or using the "heat of ablation" model. The latter assumes that ablation occurs at a fixed temperature, called the minimum ablation temperature, and that the amount of energy consumed per unit mass of material ablated is constant and equal to the heat of ablation Q^*[Ama06]:

$$Q^* = h_w - h_s \qquad (13)$$

where h_w is the gas enthalpy at the wall and h_s is the enthalpy of the charring ablator. The heat of ablation can be fixed at a constant value or it can also vary, based on the cold wall heat flux as reported in previous works ([WC92, RT99]). Using the heat of ablation model, the recession rate can be evaluated as [DB06]:

$$\dot{s} = \frac{\dot{q}_{hw}}{\rho_s Q^*} \qquad (14)$$

Once surface recession velocity has been evaluated, the computational grid has to be reconstructed in accordance with the displacement of its nodes. Each internal point is moved accordingly to the corresponding external surface. The implemented method is a two-dimensional contracting grid scheme where the relative cell thickness and the total number of cells remain constant in each receding direction and the structured mesh can move independently

in both x and y directions. The technique is inspired by the work presented in Ref.[BH94], but the Landau coordinate transformation [Lan50] is not used here and the method is extended to two-dimensions. For the sake of completeness, we report that Blackwell and Hogan's work [BH94] was later extended to more than one dimension [HBC96], but the technique, which assumes that the heat shield behaves as an elastic isotropic solid, is not applied here.

5. SOLUTION PROCEDURE

The governing equations can be reduced to a simple vector formulation written as:

$$\frac{\partial}{\partial t} \int_v \mathbf{W} dV + \int_s \mathbf{F} \cdot \mathbf{n} dS - \int_s \mathbf{F}_s \cdot \mathbf{n} dS = \int_v \mathbf{\Omega} dV \quad (15)$$

where

$$\mathbf{W} = \begin{pmatrix} E_a \\ \rho_s \\ \phi\rho_g \end{pmatrix}; \qquad \mathbf{F} = \begin{pmatrix} \phi\rho_g h_g \mathbf{v}_g + \dot{\mathbf{q}} \\ 0 \\ \phi\rho_g \mathbf{v}_g \end{pmatrix} \quad (16)$$

$$\mathbf{F}_s = \begin{pmatrix} E_a \mathbf{v}_s \\ \rho_s \mathbf{v}_s \\ \phi\rho_g \mathbf{v}_s \end{pmatrix}; \qquad \mathbf{\Omega} = \begin{pmatrix} 0 \\ \dot{m}_s \\ \dot{m}_g \end{pmatrix} \quad (17)$$

It is important to observe that in Eq. (15) several continuity equations for the solid phase have to be taken into account depending on the number of resin components that undergo the pyrolysis process. The integral equations system defined in Eq. (15) is discretized using a finite volumes method as follows:

$$\frac{\mathbf{W}^{k+1}V^{k+1} - \mathbf{W}^k V^k}{\Delta t} =$$
$$= -\sum_i (F_i S_i)^{k+\alpha} + \sum_i (F_{s,i}S_i)^{k+\alpha} + (\mathbf{\Omega}V)^{k+\alpha} =$$
$$= \mathbf{R}^{k+\alpha} \quad (18)$$

where k is the time-step index and variable α can take the values 1 or 0.5 depending on the desired time accuracy. Eq. (18) is a non-linear algebraic system that we solve using the iterative Newton-Raphson method:

$$\left\{ \frac{V^{k+1}}{\Delta t}\mathbf{I} - \alpha \left[\left(\frac{\partial \mathbf{R}}{\partial \mathbf{W}} \right)^{k+\alpha} \right]^{it} \right\} (\Delta \mathbf{W}^{k+1})^{it+1} =$$
$$= -\frac{(\mathbf{W}^{k+1})^{it} V^{k+1} - \mathbf{W}^k V^k}{\Delta t} + (\mathbf{R}^{k+\alpha})^{it}$$
$$+ \alpha \left[\left(\frac{\partial \mathbf{R}}{\partial V} \right)^{k+\alpha} \right]^{it} \Delta V^{k+1} \quad (19)$$

where the superscript it is the iterations counter. When the difference $(\Delta \mathbf{W}^{k+1})^{it+1} = (\mathbf{W}^{k+1})^{it+1} - (\mathbf{W}^{k+1})^{it}$ drops below a certain tolerance, the solution is saved and the simulation is free to advance in time. The time step Δt can be modified in order to speed up the convergence of the residuals. In particular, we set an initial value of Δt

that during the simulation can be increased or decreased depending on the total number of iterations needed to reach convergence within the inner iteration step.

The system is solved iteratively using a PGMRES (Pre-Conditioned Generalized Minimum Residual) method and ILU (Incomplete Lower Upper) factorization. The pre-conditioner can strongly reduce the number of iterations that are needed to reach convergence, but it may have a negative effect on the Jacobian matrix, the "fill-in" phenomenon. If the ILU factorization has a level of fill-in equal to zero, then the pattern of the Jacobian matrix is equal to the LU pattern and both computational costs and memory requirements remain low. However, L and U are usually dense matrices, so that, to have a more efficient factorization, we should allow a level of fill-in greater than zero. In our numerical code, the fill-in level is controlled by two different parameters that control the minimum admissible magnitude of the elements in the LU factorization (small values are dropped) and the maximum level of fill-in, respectively [Saa00]. The presence of the pyrolysis gas requires a high level of fill-in and a small dropping tolerance within the ILU factorization, because the pyrolysis gas density may be orders of magnitude smaller with respect to the other conservative variables. This particular setting of the parameters that control the ILU factorization rises the computational and memory costs and it can make simulations accounting for the pyrolysis gas computationally expensive.

6. NUMERICAL RESULTS

In this section, we show some test cases to demonstrate that the ablative module works properly and that it is able to produce accurate results that are consistent with numerical simulations available in the literature. Space- and time-accuracy verification tests, which are not shown here for lack of space, have been carried out and have shown that the code is second order accurate in space and first or second order accurate in time, depending on the choice of the parameter α (see Eq. (18)), also when the grid is contracting.

6.1. Test 1: Two-dimensional test case with pyrolysis and ablation

In this section, the atmospheric reentry of the Mars Pathfinder vehicle has been simulated in order to observe the thermal behaviour of the ablative material. The material considered is the SLA-561V [TPS05]. The computational domain consists of the forebody part of the Mars Pathfinder entry system [MCCT99] and it is discretized using 203 cells in the tangential direction and 51 cells in the radial direction. As we assume axial symmetry, only half part of the TPS is simulated. The boundary condition at the gas/solid interface is a heat flux distribution that changes in time, $q(\xi, t)$. The $q(\xi, t)$ distribution is obtained combining the results given in [MCCT99]
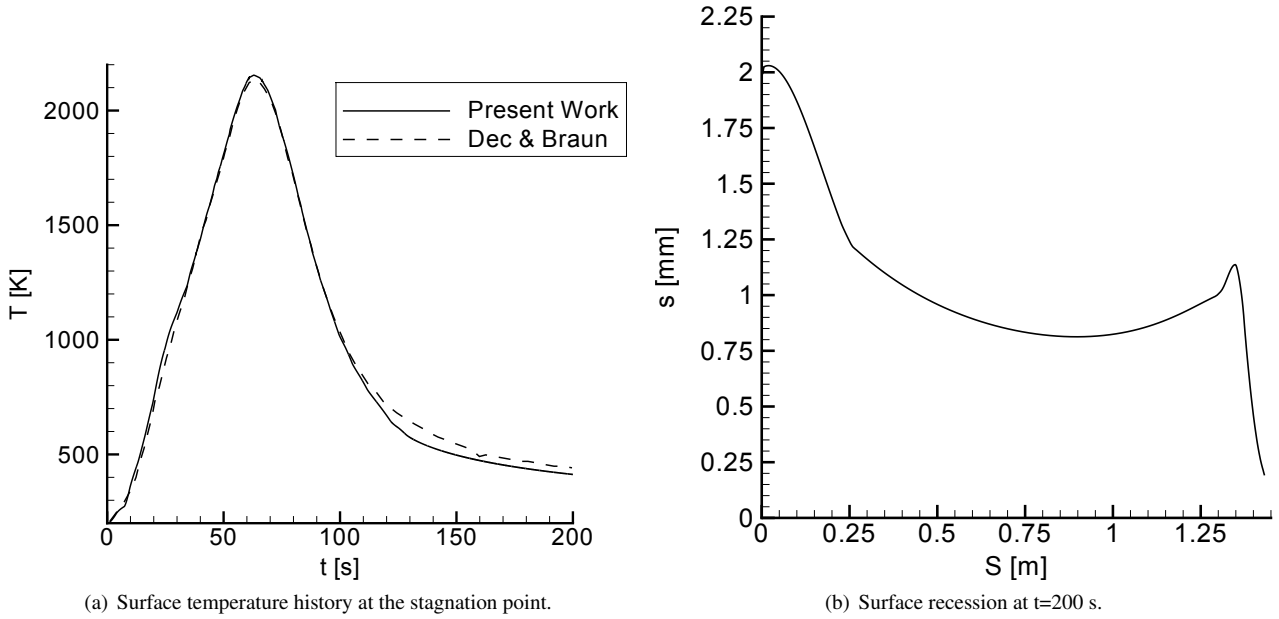
(a) Surface temperature history at the stagnation point.

(b) Surface recession at t=200 s.

Figure 1. Computed surface temperature and recession for the MarsPathfinder reentry.

and [DB06]. Noting that the heat flux distributions computed in [MCCT99] have approximately the same shape regardless of the magnitude, we derive a shape function $f(\xi) = q(\xi)/q_{st}$, where q_{st} is the stagnation heat flux. Using the heat flux rate $q_{st}(t)$ given in [DB06], we estimate the heat flux distribution rate as $q(\xi, t) = q_{st}(t)f(\xi)$. Additional boundary conditions are axial symmetry at the TPS axis and adiabatic wall conditions on the remaining two sides. We simulate a time interval of 200 s, with initial $\Delta t = 0.125$ s.

The thermal protection system can pyrolyze and recede and the heat of ablation model is used to evaluate the recession rate. The minimum ablation temperature $T_{abl_{min}}$ is 923 K, as reported in [TPS05]. The initial temperature and pressure are assumed to be 173 K and 600 Pa, respectively. It has to be noted that the pyrolysis gas is neglected due to the lack of a corresponding gas pressure history at the wall. As explained in [MCCT99], the heat flux is the highest at the stagnation point, undergoes a decrease along the stream length and increases again at the shoulder. In Fig. 1(a), the computed surface temperature history at the stagnation point is compared with Dec and Braun's results[DB06], where the surface recession is not accounted for. The results are in very good agreement, especially at the peak heating. The temperature difference that appears after 100 s is probably due to the fact that we account for recession in our simulation. The recession distribution along the streamlength at t=200 s is shown in Fig. 1(b). The maximum ablation predicted in the stagnation area is approximately 2.2 mm while at the shoulder the material recedes 1.14 mm.

6.2. Test 2: Two-dimensional test case with in-depth gas generation and wall recession

In this section we simulate the flowfield about a sphere with the same curvature radius of the Stardust capsule (R=22.86 cm)[OCT99] to show the capability of the computational tool to describe the behaviour of the pyrolysis gas inside the ablator. We assume axial symmetry and we consider the re-entry point at an altitude of 81 km, that is 34 s after atmospheric entry. The heat shield material is the Phenolic Impregnated Carbon Ablator (PICA), as described in [TJR$^+$96]. The computational grid consists of 125 cells in the radial direction and 50 cells in the tangential direction. The heat shield thickness is constant and equal to 5.82 cm. To define the solid/fluid boundary conditions for both the energy and pyrolysis gas equations, a CFD solution is generated using the freestream conditions reported in Table 2[OCT99] and assuming a non-catalytic radiative adiabatic wall. We also assume that the heat flux and pressure distributions at the wall (Fig. 2) remain constant during the time interval between the first and the second trajectory point that is set at 42 s at an altitude of 71.92 Km [OCT99]. Therefore, we simulate a time interval of 8 seconds with initial $\Delta t = 0.01$ s. Additional boundary conditions are axial symmetry at the TPS axis and adiabatic and impermeable wall conditions on the remaining two sides. The initial conditions

Table 2. Freestream flow conditions used for test #2[OCT99].

t [s]	h [km]	V_{rel} [m/s]	ρ [kg/m^3]	T [K]
34	81.64	12590.4	$9.63 \cdot 10^{-6}$	216.93

(a) Convective surface heat flux distribution.
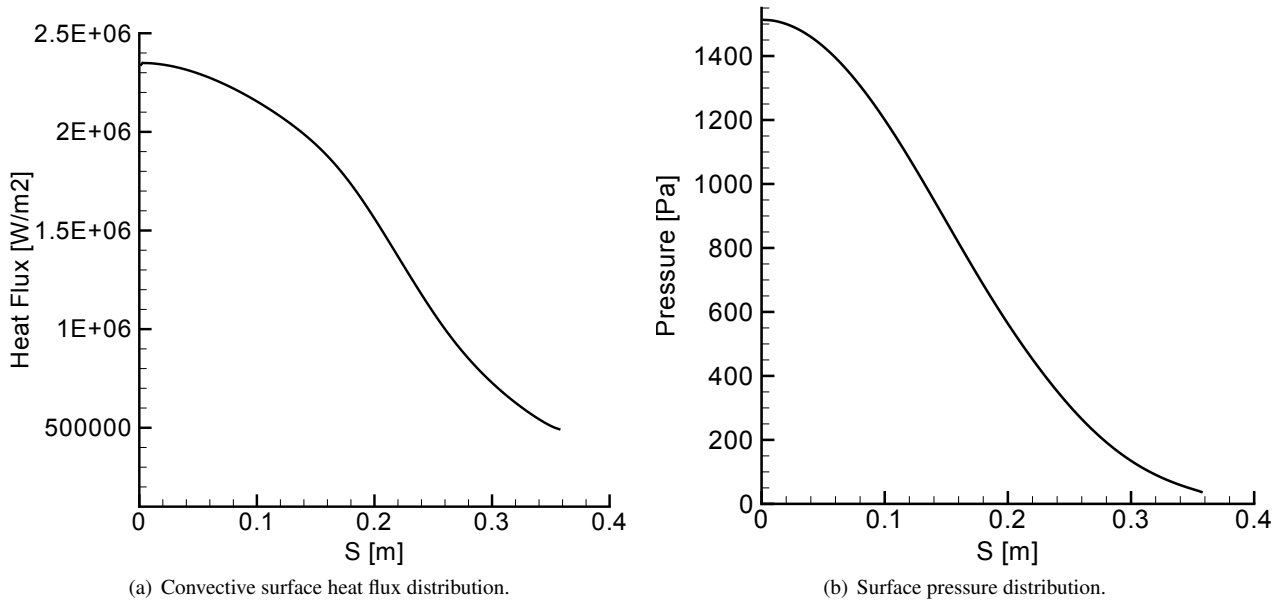

(b) Surface pressure distribution.

Figure 2. Prescribed boundary conditions at the gas/solid interface for test #2.

(a) Pyrolysis gas streamlines.

(b) Pyrolysis gas pressure, p [Pa], at t=42 s.

(c) Pyrolysis gas average velocity, v_g [m/s] at s=42 s.

(d) Pyrolysis gas density, ρ_g [Kg/m^3] at t=42 s.
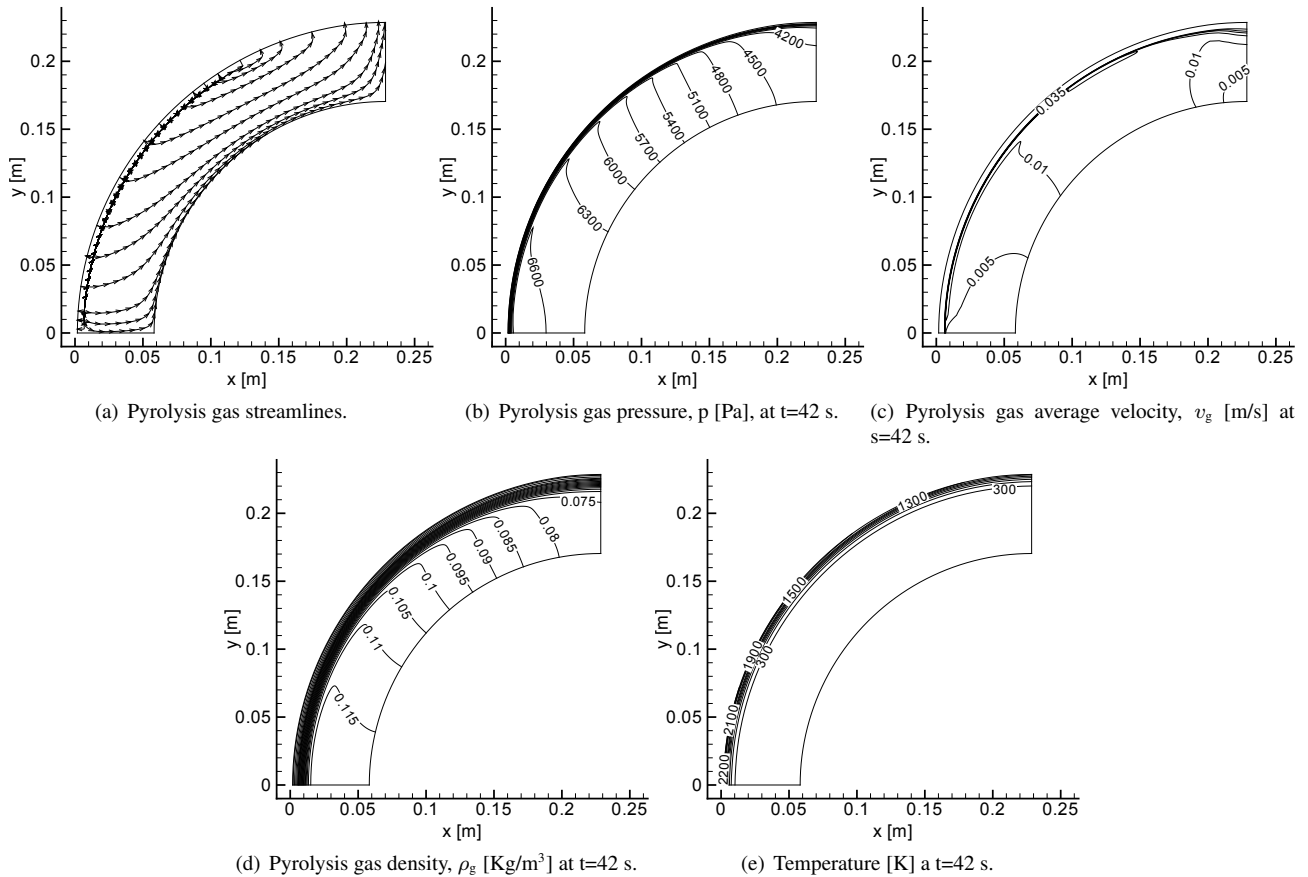

(e) Temperature [K] a t=42 s.

Figure 3. Pyrolysis gas streamlines and pressure, velocity, density and temperature distributions in the heat shield.

inside the ablator are T=216 K, p=0.602 Pa and ρ_g=1.e-5 kg/m^3. The gas generated inside the ablator as the resin decomposes is assumed to fill the material pores and, in the simulation, the corresponding pressure can be evalu-

ated using the perfect gas law. The heat shield recession has been modeled using the heat of ablation model. The minimum ablation temperature is set to 1500 K, as reported in [DB06]. Clearly, this is not an accurate simula-
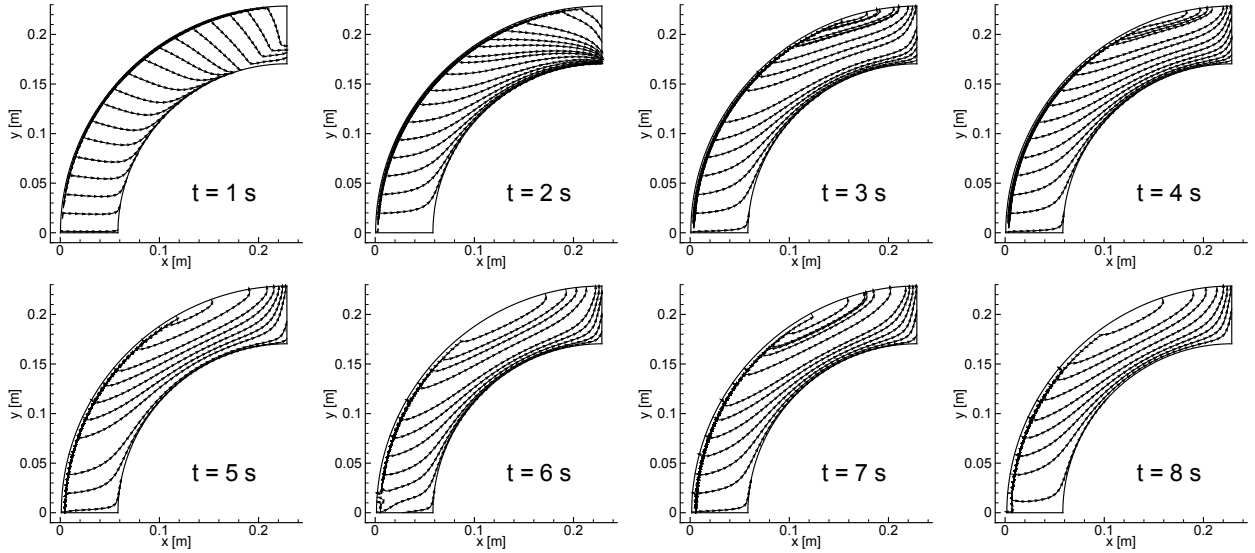
(a) Pyrolysis gas streamlines at different times.
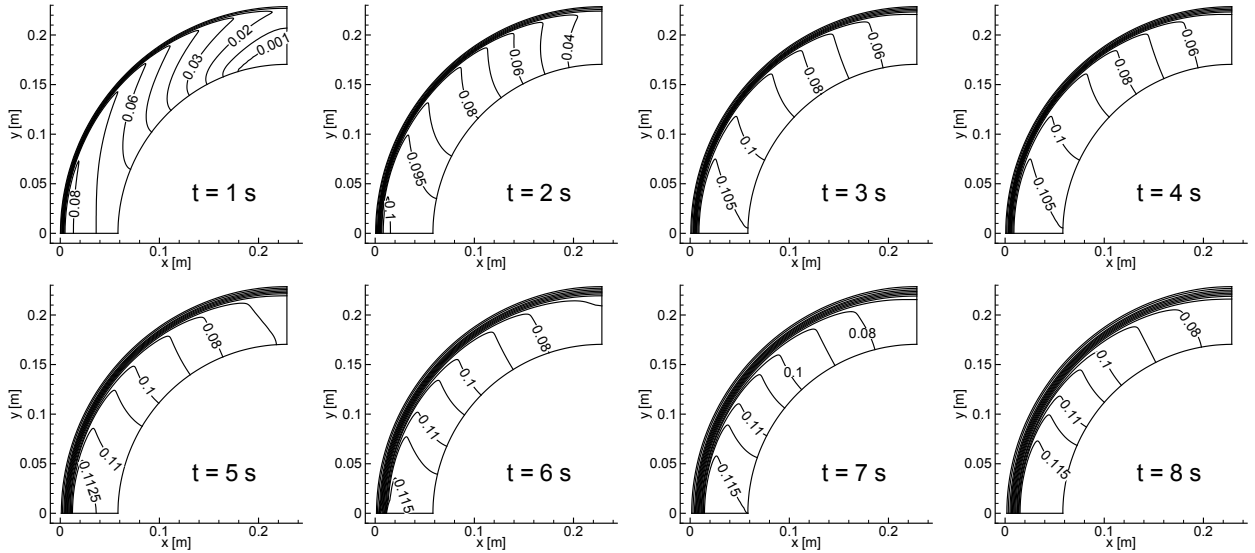
(b) Pyrolysis gas density, $\rho_g[kg/m^3]$, at different times.

Figure 4. Pyrolysis gas streamlines and density at different times.

tion of the real reentry conditions of the Stardust capsule, as we start the computation in the heat shield without considering the first 34 seconds of flight in the atmosphere and we do not account for the coupling with the external flowfield. Our aim is to show the capability of our simulation tool to predict the multi-dimensional behaviour of the pyrolysis gases inside the TPS and to demonstrate that multi-dimensionality is important in the prediction of pressure and gas density distributions inside ablating heat-shields. In Fig. 3(b) we show the pyrolysis gas pressure distribution after 8 seconds of simulation. A region of strong pressure gradients directed inwards in the radial direction occupies a layer about 4 mm thick along the external surface of the ablator. These pressure gradients are responsible for the outflow of the pyrolysis gas from the TPS towards the external flowfield. Immediately below

such an external layer, the sign of the pressure gradient component in the radial direction changes and the pyrolysis gas flows towards the inner part of the TPS. This phenomenon occurs up to an azimuthal angle of about 60°. Above this angle, the pyrolysis gas doesn't enter in the ablator, but it is directly ejected in the external flowfield. The pyrolysis gas streamlines and the magnitude of their speed are shown in Fig. 3. The pyrolysis gas expulsion layer is clearly visible, but one can also see that below it the pyrolysis gas initially flows towards the interior of the ablator and then, since the back face of the TPS is assumed to be impermeable, it deviates tangentially and is finally expelled at the shoulder of the heat-shield. The exit speed of the pyrolysis gas out of the ablator ranges from 3.0 to 3.6 m/s and its largest value is not at the stagnation point, but at about 52° degrees above the symmetry
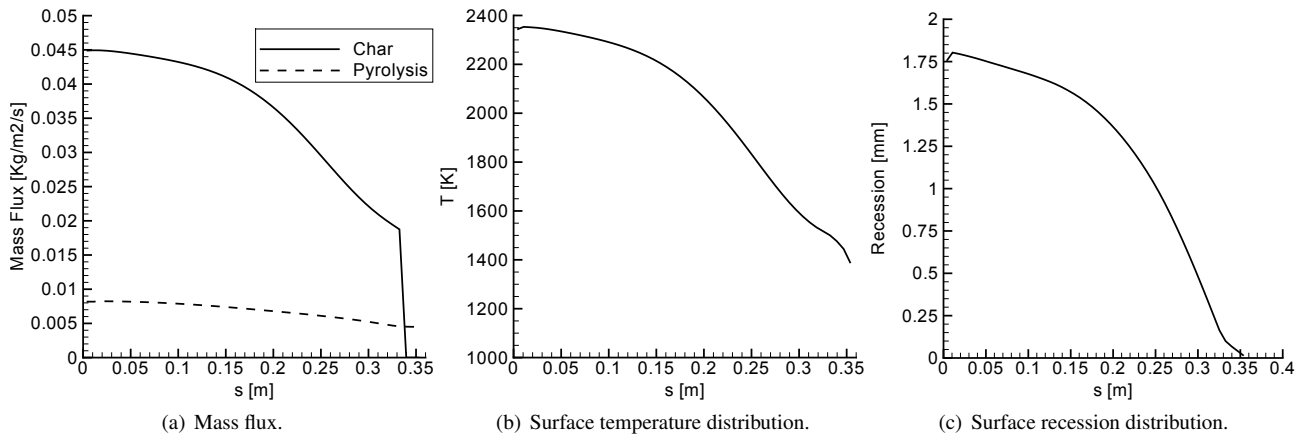
(a) Mass flux.   (b) Surface temperature distribution.   (c) Surface recession distribution.

Figure 5. Computed mass flux, surface temperature and surface recession distributions after 8 seconds of simulation.

axis. Internally, the pyrolysis gas speed is about 1 cm/s in most part of the ablator. In Figs. 3(d) and 3(e) we show the pyrolysis gas density and the temperature distribution inside the ablator. The pyrolysis gas is generated close to the high-temperature wall where the material decomposes. A part of it is expelled, but another part quietly moves towards the back face of the heat shield and it is finally expelled at the shoulder of the TPS. It is interesting to consider the time evolution of the pyrolysis gas streamlines and density during the 8 seconds of the simulation, as we show in Figs. 4(a) and 4(b). Initially, the pyrolysis gas that is produced near the solid/fluid interface is partially expelled and partially travels towards the interior of the ablator, moving in the radial direction. The gas production is the largest near the stagnation point and thus, at the beginning, the pyrolysis gas mostly fills the ablator underneath the stagnation region. When the gas reaches the back-face of the TPS, it is forced to deviate tangentially due to the impermeability boundary condition. Therefore, after a few seconds, part of the pyrolysis gas generated near the stagnation region contributes to filling the ablator in the shoulder region also. When the pyrolysis gas has filled the TPS shoulder region, it is forced to move towards the external wall of the heat shield by the impermeability boundary condition that has been imposed at the lateral surface of the TPS. Therefore, after some time, part of the TPS starts to expel gas that was generated in the hot layer close to the surface, but another part, far from the stagnation region, expels gas that was produced near the stagnation region and that travelled inside the TPS towards low pressure zones.

In Fig. 5(a), we show the char and pyrolysis gas mass fluxes distributions along the wall after 8 seconds of simulation. The major contribution to the blowing mass flux at stagnation point is due to the char. In particular, the char mass flux at the stagnation point is 0.0445 Kg/m^2/s, while the pyrolysis gas mass flux is 0.0089 Kg/m^2/s. These values are consistent with those reported in the literature[CM04, CM05a]. The wall temperature distribution is shown in Fig. 5(b). The maximum wall temperature is reached at the symmetry axis and it is about 2350 K. The radial recession of the surface can be observed in Fig. 5(c). Ablation is large close to the stag-

nation point, where the TPS reaches the maximum wall temperature during the simulated time interval, while at the edges of the sphere the minimum ablation temperature is not reached and the shape of the heat shield remains unchanged. As it can be observed in Fig. 5(c), the decrease in recession with the curvilinear coordinate is very smooth. This trend is due to the heat flux distribution along the wall: since the heat flux decreases gradually as we move towards the edge of the computational domain, the recession also has to change slowly.

7. CONCLUSIONS

In this paper, we introduce a fully implicit 2-D numerical simulation tool capable of simulating the behaviour of an ablative charring material during atmospheric reentry. The code can handle ablative materials with very different thermochemical properties, allowing a wide field of applications, and it is able to study the pyrolysis process by including both the decomposition of the matrix and the generation of pyrolysis gas inside the pore space. The computational grid can move to simulate the recession of the material. To obtain the recession rate of the surfaces, various ablation models can be chosen depending on the available data. The code was tested on several domains made up of different ablative materials. The comparison with numerical and experimental results showed a generally good agreement, provided that the time step is sufficiently small when the pyrolysis gas is considered. The solid solver is coupled with a CFD solver for high temperature hypersonic flows, but we do not show results here because the thermo-chemical modelling of gas surface interactions has not been validated yet.

The multi-dimensional analysis of the pyrolysis gas behaviour enables the prediction of the pore pressure that has to be checked in order to avoid in-depth damage of the solid. In addition, it can suggest improvements to the physical models that are used to simulate thermal protection systems. For example, the results that we show in Sec. 6.2 pose a question on the correctness of the hypothesis of thermal equilibrium between the solid and the

gaseous phases in the ablator, as we demonstrated that part of the pyrolysis gases generated in the hot external layer of the TPS travel inside the heat shield from high pressure regions near the stagnation point to low pressure zones at the shoulder of the ablator. The computed speed of the pyrolysis gas inside the ablator is not particularly large (about 1 cm/s) in the test case that we considered, but, still, the question arises whether two separate energy equations for the solid material and the pyrolysis gases would be appropriate to simulate the possible internal heating of ablator due to the in-depth flow of hot pyrolysis gases.

8. ACKNOWLEDGMENTS

REFERENCES

[ABE08] A. J. Amar, B. F. Blackwell, and J. R. Edwards. One Dimensional Ablation using a Full Newton's Method and Finite Control Volume Procedure. *Journal of Thermopysics and Heat Transfer*, 22(1):71–82, Jan.-Mar. 2008.

[ABE09] A. J. Amar, B. F. Blackwell, and J. R. Edwards. Development and verification of a one-dimensional ablation code including pyrolysis gas flow. *Journal of Thermopysics and Heat Transfer*, 23(1):59–71, Jan.-Mar. 2009.

[ACK11] A. Amar, N. Calvert, and B. Kirk. Development and verification of the charring ablating thermal protection implicit system solver. In *49th AIAA Aerospace Sciences Meeting and Exhibit*, Orlando, FL, January 2011. AIAA Paper 2011-144.

[Ama06] A. J. Amar. Modeling of One-Dimensional Ablation with Porous Flow Using Finite Control Volume Procedure. Master's thesis, North Carolina State University, 2006.

[BH94] B. F. Blackwell and R. E. Hogan. One-dimensional ablation using landau transformation and finite control volume procedure. *Journal of Thermophysics and Heat Transfer*, 8(2):282–287, 1994.

[Bla88] B. F. Blackwell. Numerical prediction of one-dimensional ablation using a finite control volume procedure with exponential differencing. *Numerical Heat Transfer*, 14(1):17–34, 1988.

[Cla73] R. K. Clark. An analysis of a charring ablator with thermal nonequilibrium, chemical kinetics, and mass transfer. Technical Note NASA-TN-D-7180, NASA LaRC, Hampton, VA, USA, June 1973.

[CM99] Y. K. Chen and F. S. Milos. Ablation and thermal response program for spacecraft heatshield analysis. *Journal of Spacecraft and Rockets*, 36(3):475–483, May-June 1999.

[CM01] Y. K. Chen and F. S. Milos. Two-dimensional implicit thermal response and ablation program for charring materials. *Journal of Spacecraft and Rockets*, 38(4):473–481, Jul.-Aug. 2001.

[CM04] Y.-K. Chen and F. S. Milos. Finite-rate ablation boundary conditions for a carbon-phenolic heat-shield. In *37th AIAA Thermophysics Conference*, Portland, OR, June-July 2004. AIAA Paper 2004-2270.

[CM05a] Y. K. Chen and F. S. Milos. Navier-stokes solutions with finite rate ablation for planetary mission earth reentries. *Journal of Spacecraft and Rockets*, 42(6):961–970, Nov-Dec. 2005.

[CM05b] Y.-K. Chen and F. S. Milos. Three-dimensional ablation and thermal response simulation system. In *38th AIAA Thermophysics Conference*, Toronto, June 2005. AIAA Paper 2005-5064.

[CMG10] Y. K. Chen, F. S. Milos, and T. Göçen. Validation of a three-dimensional ablation and thermal response simulation code. In *10th AIAA/ASME Joint Thermophysics and Heat Transfer Conference*, Chicago, IL, June 2010. AIAA-2010-4645.

[Dar56] H. Darcy. *Les fontaines publiques de la ville Dijon*. Dalmont, Paris, France, 1856.

[DB06] J. A. Dec and R. D. Braun. An approximate ablative thermal protection system sizing tool for entry system design. In *44th AIAA Aerospace Sciences Meeting and Exhibit*, Reno, NV, USA, Jan. 2006. AIAA. AIAA Paper 2006-0780.

[Gol65] H. E. Goldstein. Kinetics of nylon and phenolic pyrolysis. Technical report, Lockheed Missiles and Space Company, Sunnyvale, CA, 1965.

[HBC96] R. E. Hogan, B. F. Blackwell, and R. J. Cochran. Application of moving grid control volume finite element method to ablation problems. *Journal of Thermophysics and Heat Transfer*, 10(2):312–319, 1996.

[Lan50] H. G. Landau. Heat conduction in a melting solid. *Quarterly of Applied Mathematics*, 8(1):81–94, 1950.

[MB08] A. Martin and I. D. Boyd. Simulation of pyrolysis gas within a thermal protection system. In *40th AIAA Thermophysics Conference*, Seattle, Washington, June 23-26 2008. AIAA-2008-3805.

[MB09a] A. Martin and I. D. Boyd. Implicit implementation of material response and moving meshes for hypersonic re-entry ablation. In *47th AIAA Aerospace Sciences Meeting including The New Horizons Forum and Aerospace Exposition*, Jan. 2009. AIAA Paper 2009-670.

[MB09b] A. Martin and I. D. Boyd. Strongly coupled computation of material response and nonequilibrium flow for hypersonic ablation. In *41th AIAA Thermophysics Conference*, San Antonio, TX, June 2009. AIAA Paper 2009-3597.

[MB10] A. Martin and I. D. Boyd. Mesh tailoring for strongly coupled computation of ablative material in nonequilibrium hypersonic flow. In *10th AIAA/ASME Joint Thermophysics and Heat Transfer Conference*, Chicago, IL, June-July 2010. AIAA Paper 2010-5062.

[MCCT99] F. S. Milos, Y.-K. Chen, W. M. Congdon, and J. M. Thornton. Mars pathfinder entry temperature data, aerothermal heating and heatshield material response. *Journal of Spacecraft and Rockets*, 36(3):380–391, May-Jun. 1999.

[MR68] C.B. Moyer and R.A. Rindal. An analysis of the coupled chemically reacting boundary layer and charring ablator, part ii: Finite difference solution for the in-depth response of charring materials considering surface chemical and energy balances. Technical Report NASA CR-1061, NASA, June 1968.

[NB06] D. A. Nield and A. Bejan. *Convection in Porous Media*. Springer, third edition edition, 2006.

[OCT99] D. Olynick, Y.-K. Chen, and M. Tauber. Aerodynamics of the stardust sample return capsule. *Journal of Spacecraft and Rockets*, 36:442–451, 1999.

[RT99] D. J. Rasky and H. K. Tran. Low-cost entry systems for future planetary exploration missions. *Acta Astronautica*, 45(4):347–355, August 1999.

[Saa00] Y. Saad. *Iterative Methods for Sparse Linear Systems*. SIAM, Society for Industrial and Applied Mathematics, 2nd ed. edition, 2000.

[TJR⁺96] H. Tran, C. Johnson, D. Rasky, F. Hui, Y.-K. Chen, and M. Hsu. Phenolic impregnated carbon ablators (pica) for discovery class mission. In *31st AIAA Thermpophysics Conference*, New Orleans, LA, June 1996. AIAA Paper 96-1911.

[TPS05] Tpsx, thermal protection systems expert material property database v4.0. *NASA Ames, San Jose, CA*, 2005.

[WC92] S. D. Williams and Donald M. Curry. Thermal protection materials - thermophysical property data. NASA Reference Publication NASA-RP-1289, NASA, Dec. 1992.

[Whi86] S. Whitaker. Flow in porous media i: A theoretical derivation of darcy's law. *Transport in Porous Media*, 1:3–25, 1986.

[WM14] H. Weng and A. Martin. Multi-dimensional modeling of pyrolysis gas transport inside charring ablative materials. *Journal of Thermophysics and Heat Transfer*, 28(4):583–597, 2014.